Journal of Power Sources 517 (2022) 230677

Contents lists available at ScienceDirect

Journal of Power Sources

journal homepage: www.elsevier.com/locate/jpowsour

Dual-feature photobioanodes based on nanoimprint lithography for photoelectric biosupercapacitors

O. Aleksejeva [a,*], N. Nilsson [b], V. Genevskiy [a], K. Thulin [b], S. Shleev [a]

[a] Department of Biomedical Science, Malmö University, 205 06, Malmö, Sweden
[b] Obducat Technologies AB, 223 63, Lund, Sweden

HIGHLIGHTS

- Nanoimprinted gold substrates were used to design photobioanodes.
- Both supercapacitive and conventional photobioanodes were designed and tested.
- Dual-feature photobioanodes provided low open circuit potential at ambient light.
- Mediator-less photoelectric biosupercapacitor was fabricated.
- Photobiodevice provided remarkably stable high open circuit voltage at day light.

ARTICLE INFO

Keywords:
Biosupercapacitor
Photosynthetic electricity
Thylakoid membranes
Nanoimprint lithography
Ambient light

ABSTRACT

Direct transformation of solar energy into electrical energy by means of biological photosynthesis is considered as an attractive option for sustainable electrical energy production. Thylakoid membranes, the site of photosynthesis, are regarded as a promising biological material for the development of photoelectric biodevices, which produce electrical power consuming only light energy as oxygen evolves at photobioanode upon irradiation and biocathode converts it back to water. Therefore, in this work dual-feature photobioanode based on nanoimprinted gold substrates modified with thylakoids in combination with a capacitive part made of a planar gold substrate coated with a conductive polymer was designed and evaluated, providing open-circuit potential of −0.21 V *vs.* Ag|AgCl|KCl_{sat} and a capacitance of *ca.* 60 F m^{-2} both at ambient light and artificial illumination of 400 W m^{-2}. Combination of thylakoid based dual-feature photobioanode with bilirubin oxidase modified transparent and capacitive indium tin oxide biocathode resulted in a photoelectric biosupercapacitor with remarkable characteristics at ambient light, *viz.* an open-circuit voltage as high as 0.74 V, which was stable upon charge-discharge cycles during *ca.* 2 h.

1. Introduction

Electrical power production using only radiant energy without consumption of any (bio)fuels has become an attractive alternative for fully sustainable energy generation [1–3]. Solar energy is the most abundant, accessible and inexhaustible energy source amongst other renewable energy sources [2]. Photobioelectrical systems are arising green energy producing technologies, where photosynthetic biomaterials in combination with an electronic conductor are used to directly convert solar energy into electrical energy [3]. Various photosynthetic biological species, both of subcellular and cellular characters, are being employed to transform solar energy into the electrical energy, such as photosynthetic reaction centers (PSI and PSII), thylakoid membranes, chloroplasts, cyanobacteria or green algae [3,4], having their advantages and disadvantages depending on the particular application. Thylakoids are regarded as favorable candidates for biosolar cells manufacturing due to a higher stability, since the photosynthetic protein complexes are retained in their native environment, allowing several electron transfer pathways [3,5]. Thylakoid membranes, the site of photosynthesis, are accommodated inside the lipid envelope of chloroplasts. Chloroplasts have established self-repair mechanisms against photodamage and reactive oxygen species, however, they have been less investigated for photosynthetic electricity production compared to other photobiocatalysts [3,6].

* Corresponding author.
E-mail address: olga.aleksejeva@mau.se (O. Aleksejeva).

https://doi.org/10.1016/j.jpowsour.2021.230677
Received 2 August 2021; Received in revised form 21 September 2021; Accepted 23 October 2021
Available online 3 November 2021

A key challenge in the design of photobioelectrodes is to boost the electrical communication between biocatalysts and electrode surface. Therefore, various nanomaterials, such as carbon nanotubes [5,7], nanowires [8], gold nanoparticles [9,10], and even two-dimensional materials, such as graphene [11,12], were combined with photosynthetic catalysts, and their enhanced performance was demonstrated in comparison to the systems without nano-structuration. However, these approaches rely on secondary connection between photobiocatalyst and electrode [13], resulting in irreproducible geometry of the electrode surface and, hence, wavy electrochemical response. However, only a few works were performed using nanoimprinted electrodes, which assure well-controlled nanostructured geometry [14] and allow efficient accommodation of photo-biocatalysts inside the three-dimensional nanostructures [15] for photosynthetic electricity production [13,16]. These studies have demonstrated the feasibility of an efficient deposition of photo-biocatalysts on micro-patterned electrodes aimed to increase the contact area between the biological species and the anodes. For instance, DongHyun Ryu et al. [13] employed photolithography to fabricate micro-pillar patterned anodes to accommodate thylakoids. A different approach was used by Samson Patole et al. [16] who took advantages of the self-assembled monolayer formation of alkylthiolates on gold surface to immobilise light-harvesting complexes. The patterning was performed by interference lithography using an ion laser which allowed to easily modulate both the periodicity and the width of the pattern.

In this study, a third method was used, *viz.*, nanoimprint lithography (NIL). Unlike the majority of other patterning techniques, NIL is a high throughput, cost-effective and versatile process. Traditional methods operating in the nanofabrication field, such as e-beam lithography, photolithography or interference lithography require high energy radiation, complex optics and extremely expensive machines for fabrication [17,18]. With NIL, patterns with features <100 nm size and high aspect ratios (up to 10) have been reported to be achievable at a fraction of the cost of photolithography [19–22]. Besides, combination of NIL and etching processes has shown the capability of fabricating pillar structures with extremely high aspect ratios, greater than 50:1 [23]. NIL working principle is fairly simple. Briefly, a rigid stamp containing a nano- or micro-featured pattern is pressed under controlled temperature and pressure conditions onto a thin polymeric pre-heated (or UV-curable) resist, deposited on top of a substrate. With such a simple process, NIL offers a broad range of polymeric materials to be directly functionalised rather than to be used as sacrificial masks for etching [24]. In fact, imprinted polymer films found a vast application in different fields, where only a modified functional layer is required and where the standard methods such as e-beam lithography and photolithography are costly and do not provide sufficient throughput [25]. These characteristics gives NIL a significant edge on photolithography, allowing the fabrication of patterned and flexible polymeric sheets, not only on flat surfaces but also in the presence of curvatures or sharp edges [15,26], an imperative attribute for electronics, optics and in particular biodevices, where the ergonomics is a vital characteristic [27,28].

Therefore, in this work we introduce a novel design of dual feature NIL based photobioanode consisting of gold electrodes modified with thylakoids for photosynthetic electricity production in combination with a capacitive part made of a planar gold substrate coated with a conductive polymer for enhancement of charge storing capabilities, taking advantage of the earlier disclosed principle of simultaneous energy conversion and storage in a singular module [29,30], as well as a biodevice made thereof. Combination of thylakoid based dual feature bioanode with indium tin oxide (ITO) electrode decorated with ITO nanoparticles and modified with bilirubin oxidase resulted in a photoelectric biosupercapacitor with remarkable characteristics functioning at day light conditions.

2. Materials and methods

2.1. Chemicals and materials

$Na_2HPO_4{\cdot}2H_2O$, $NaH_2PO_4{\cdot}H_2O$, NaCl, $MgCl_2$, KCl, NaOH, H_2SO_4 (98%), $K_3[Fe(CN)_6]$, $K_4[Fe(CN)_6]$, EDOT (3,4-ethylenedioxythiophene), gelatin from porcine skin, *p*-benzoquinone were purchased from Sigma-Aldrich (St. Louis, USA). Tris(hydroxymethyl)aminomethane was obtained from Kebo AB (Stockholm, Sweden). Glycine was obtained from Fisher Chemical (Leics, United Kingdom). Sucrose was purchased from BDH Laboratory supplies (Poole, England). 99.5% ethanol was obtained from CCS Healthcare AB (Malmö, Sweden). All chemicals were of analytical grade and used without further purification. All solutions were prepared using water purified with the PURELAB UHQ II system from ELGA Labwater (High Wycombe, United Kingdom). Indium tin oxide (ITO)-coated poly(ethylene terephthalate) (PET) 60 Ω/sq was purchased from Sigma Aldrich, ITO nanoparticles (In_2O_3:SnO_2 = 90:10, 20–70 nm) were obtained from Sky Spring Nanomaterials Inc. (Houston, USA).

2.2. Biocatalysts

2.2.1. Thylakoid membranes

Thylakoid membranes (TMs) were isolated from spinach leaves, as described previously [31], with the only difference that 10 mM pH 7.4 Tris-Glycine buffer was used instead of 10 mM pH 7.4 Tricine buffer. The TM suspension was stored at −80 °C. The chlorophyll concentration was determined using acetone extraction method according to Arnon et al. [32]. Briefly, 10 μl of freshly isolated thylakoids were suspended in 1 ml of 80% (*v/v*) acetone and centrifuged at 3000×*g* for 3 min to retain supernatant. The absorbance of the supernatant was measured at 645 nm and 663 nm, and the chlorophyll concentration was calculated using following equation:

$$C_{Chl}\ (\text{mg ml}^{-1}) = (8.02A_{663} + 20.2A_{645})/10 \quad (1)$$

The chlorophyll concentration of isolated thylakoids was determined to be 0.47 mg ml^{-1}. A microscope image of isolated thylakoid membranes is shown in Supporting Fig. S1.

Oxygen evolving activity of thylakoids was measured using a Clark-type O_2 electrode from Hansatech Ltd. (Norfolk, England) in PBS pH 7.4, containing thylakoid membranes, upon addition of 3 mM $K_3[Fe(CN)_6]$ to the cell. The oxygen evolution activity was measured under irradiation of 400 W m^{-2}, resulting in 45.5 μmol $O_2/(mg_{Chl}{\cdot}h)$, Supporting Fig. S2.

2.2.2. Myrothecium verrucaria bilirubin oxidase (MvBOx)

*Mv*BOx, 3.61 mg ml^{-1} (60 μM) in 20 mM Tris buffer, 0.1 M Na_2SO_4, pH 8.0, was kindly supplied by Novozymes A/S (Bagsværd, Denmark).

2.3. Electrode fabrication and characterisation

2.3.1. Fabrication of imprinted substrates

Prior nanoimprinting the silicon master stamp was antisticked with an anti-sticking monolayer in Fiji molecular vapor deposition tool (Vactec, Heinenoord, the Netherlands) at Lund NanoLab (Lund, Sweden). The Si master stamp consists of microholes arranged in a rectangular array (pattern area 10 × 10 mm^2) with dimension of 2 μm in diameter, 2.15 μm in pitch and 60 nm in depth. The acrylate-based UV curable polymer film on polyethylene terephthalate (PET) flexible polymer substrate was adopted first to replicate the patterns from the silicon master stamp *via* Obducat EITRE® 6 nanoimprint tool (Lund, Sweden) at room temperature with a pressure of 20 bar and a UV dose of 5.4 J cm^{-2}. The UV-curing process transforms the polymer from soft and sticky to hard with a low adhesion surface, allowing easy separation from the Si stamp. After imprinting, the micro-pillars were fidelity

transferred into the UV-film, however, the microholes were actually required on the final UV films, therefore the first UV film patterned with micropillars were deposited with a carbon fluoride based releasing layer by Obducat custom built chemical vapor deposition (CVD)-antisticking equipment and then the nanoimprinting was performed between the first and second UV-film (of the same type), thereby the desired microholes were produced on the second UV-film [33]. For all imprints, deposition of the polymer films in imprint was done with roller to minimize problems with air-inclusions, and separation after UV-curing and pressure release was performed manually by a tweezer, peeling off the top film from one side to the other. It was shown that one CVD-antisticking treated UV film could be repeatedly used to produce five final microhole patterned UV films. In contrast to the antisticking layer on the Si stamp, the release layer for imprinting the two polymer substrates is several molecules thick, as it must also work as an efficient blocking layer, preventing the second substrate UV-polymer from diffusing into the first and glue the substrates together. As a final step e-beam evaporation of 5 nm titanium followed by 100 nm gold was performed on the substrates at a pressure below $2.0{\cdot}10^{-6}$ Torr in Temescal FC-2000 equipment, by Ferrotec Corporation (Livermore, CA, USA). The process of gold coated plastic substrate production by NIL is shown in Supporting Fig. S3.

2.3.2. Cleaning and characterisation of gold electrodes

Scanning electron microscopy (SEM) images of nanoimprinted gold coated plastic substrates were obtained using an EVO LS10 scanning electron microscope from Zeiss (Jena, Germany) equipped with a LaB6 filament. Imaging was done in high vacuum mode using a secondary electron detector set to 15 kV accelerating voltage and 50 pA probe current.

Atomic force microscopy (AFM) images were obtained using a Multimode VIII SPM with a Nanoscope V control unit from Bruker AXS (Santa Barbara, CA, USA). The AFM was operated in a tapping mode. All images were obtained in air and at room temperature. Rectangular silicon cantilevers with a nominal spring constant of 2 N m^{-1}. OMCL-AC240TS Olympus Cantilevers (Tokyo, Japan) were employed in all measurements. The analysis and processing of the AFM images was performed with the WSxM software package [34].

The working area of nanoimprinted and planar gold electrodes was defined to be 0.5 cm × 0.25 cm (0.125 cm^2). Electrodes were cleaned electrochemically by cyclic voltammetry in 0.5 M NaOH solution by scanning the potential from −0.2 V to −1.2 V *vs.* Ag|AgCl|KCl_{sat} (here and below all potentials are given *vs.* Ag|AgCl|KCl_{sat}), 25 scans with a scan rate 0.1 V s^{-1} [35,36], with subsequent cycling in 0.5 M H_2SO_4 from −0.2 V to 1.7 V, 25 scans with a scan rate 0.1 V s^{-1}. This procedure allowed to obtain maximally clean electrodes, as evident from cyclic voltammograms (CVs) in H_2SO_4 (an increase in Au oxide reduction peak area) and by electrochemical impedance spectroscopy (EIS) studies in PBS buffer, without damaging the gold layer. Real surface area of the electrodes was calculated from the measured electrical charge value associated with the Au oxide reduction peak, obtained by electrochemical cleaning in 0.5 M H_2SO_4 solution. Experiments with planar Au electrodes were performed for reference purposes.

2.3.3. Fabrication of ITO electrodes modified with ITO nanoparticles

A working area of 0.5 cm × 0.5 cm (0.25 cm^2) on indium tin oxide (ITO) coated polyethylene terephthalate (PET) film was selected for nano-structuring. For the nano-structuring process dispersion of 10% of ITO nanoparticles (ITOnps) in methanol was prepared and then sonicated during 20 min to ensure efficient homogenisation. To fabricate the drop-coated ITOnps electrodes, 5 μl of the dispersion was dropped onto the ITO coated PET and air-dried.

2.3.4. Biomodification of electrodes

Biomodification of electrodes with photosynthetic organelles was carried out following the procedure desribed in Ref. [37] with slight modifications. Briefly, thylakoid membranes were deposited onto a newly cleaned NIL modified and planar electrode surfaces using physical adsorption, by spreading 3 μl of thylakoids on the defined working area, and then kept at + 4 °C for *ca.* 1 h. Thereafter, 3 μl of a gelatin solution in water (2.5% *w/v*) was distributed evenly on top of the thylakoids in order to prevent leakage of the biological species from the electrode surface, resulting in Au_NIL/thylakoids and Au_planar/thylakoids electrodes. The electrodes were dried at room temperature for *ca.* 30 min prior to electrochemical investigations.

In case of biocathode 10 μl of *Mv*BOx were drop casted onto the clean electrode surface for 20 min without drying, resulting in ITO/ITOnps/*Mv*BOx electrodes.

2.3.5. Construction of dual feature anodes

To increase the charge storing capabilities of the bioanodes, biomodified Au_NIL electrodes were combined (electrically connected) with (to) poly(3,4-ethylenedioxythiophene) (PEDOT) modified planar gold electrodes, Au_planar/PEDOT, of similar dimensions. PEDOT was synthesized electrochemically by cyclic voltammetry. The electropolymerisation procedure was carried out as described previously [38]. Briefly, the electropolymerisation solution consisted of 20 mM EDOT monomer, 1 mM PEG, and 0.1 M $LiClO_4$ in water. PEG was added to ensure better solubility of EDOT. The potential was scanned from −0.2 V to 1.3 V with a scan rate of 0.05 V s^{-1}. To maintain a good interplay between capacitance and charge transfer resistance the number of cycles was optimised and found to be equal to 3.

2.4. Electrochemical measurements

Electrochemical experiments, *i.e.*, EIS, cyclic voltammetry, amperometry and potentiometry, were performed using a μAutolab Type III/FRA2 potentiostat/galvanostat from Metrohm Autolab B. V. (Utrech, The Netherlands) in an electrochemical cell with a total volume of 30 ml. Ag|AgCl| KCl_{sat} (0.199 V *vs.* NHE) and platinum wire were used as reference and counter electrodes, respectively. All electrochemical measurements were performed in air saturated 10 mM phosphate buffered saline (PBS) pH 7.4, containing 5 mM $MgCl_2$ and 10 mM NaCl. In mediated electron transfer experiments 0.6 mM PBQ (optimised value taken from Ref. [39]) was added to the electrolyte. EIS measurements were carried out with a voltage amplitude of 0.01 V over the frequency range 0.1 Hz–50 kHz at E_{dc} equal to the open circuit potential of the electrode. ZView software from Scribner Associates Inc. (Southern Pines, North Carolina, USA) was used to fit the data. All the experiments were performed at room temperature. Measurements were repeated three times and a standard deviation less than 10% was obtained.

To perform photoelectrochemical experiments under artificial illumination, a fiber optic illuminator 150 W 220 V Fiber-Lite MI-150 single gooseneck system from Vision Light Tech B.V. (Uden, The Netherlands) was used to illuminate working electrodes. The illuminator light intensity was adjusted to 400 W m^{-2} using a digital light meter DEM300 from Velleman (Gavere, Belgium). Quite low light intensity of 400 W m^{-2} was chosen because most of the world's population live in areas with insolation levels of 150–342 W m^{-2} [9], so the light intensity value used in this work as well as in earlier studies [5,9–11] on photosynthetic electricity production lies very close to the real terrestrial irradiance values.

Experiments were also performed at day light, *i.e.*, at ambient light coming through the window of the lab during day, which intensity was 10–15 times weaker compared to the artificial light source, *ca.* 30–40 W m^{-2}.

3. Results and discussion

3.1. Characterisation of gold electrodes

SEM and AFM studies of NIL gold surfaces (Au_NIL) were performed

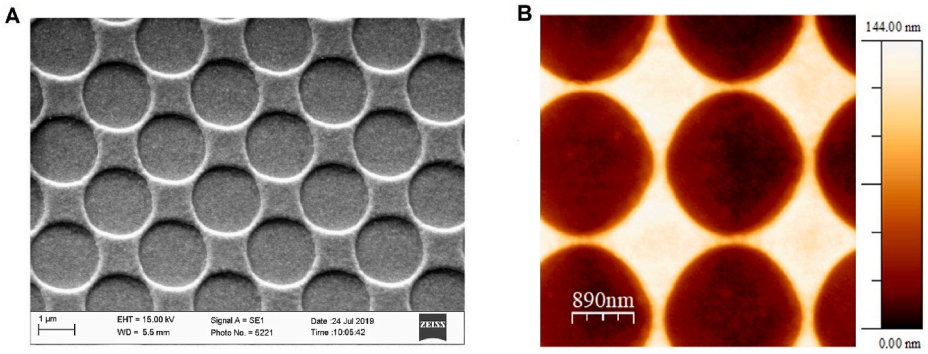

Fig. 1. SEM (A) and AFM (B) images of Au_NIL electrodes.

in order to confirm well-defined nanoimprinted structure, which dimensions were verified to be 2 μm in diameter and 60 nm in depth (Fig. 1A and B). As Au surface, especially evaporated Au, should be cleaned immediately before the biomodification, the cleaning procedure was developed based on the cleaning protocol described in Refs. [35, 36]. The main challenge was to design a gentle and effective cleaning procedure in order to preserve the gold layer intact. Upon cleaning electrodes were examined by cyclic voltammetry and EIS, evaluating peak-current potential differences and charge transfer resistance, respectively. The best results were obtained using a subsequent electrochemical cleaning in basic (0.5 M NaOH) and acidic (0.5 M H_2SO_4) solutions. The roughness factor obtained from electrochemical studies in 0.5 M H_2SO_4 was expectedly higher for Au_NIL electrodes compared to Au_planar electrodes, *viz.*, 1.7 and 1.1, respectively (Supporting Fig. S4). Cleaned electrodes were immediately modified with thylakoid membranes and used in electrochemical experiments.

3.2. Evaluation of photobioanodes

Amperometric investigations showed that electrodes modified with thylakoids demonstrated difference in photocurrent densities between NIL and planar surfaces, *ca.* 20% for direct electron transfer (DET), Fig. 2A, and *ca.* 7% for mediated electron transfer (MET), Fig. 2B. NIL contributes to a larger real surface area ensuring higher photobiocatalyst loading, therefore, higher photosynthetic currents were expected. Accomodation of thylakoids inside the micro-holes may also contribute to the enhanced contact between the photobiocatalyst and electrode surface, resulting in more efficient ET. Storage stability of Au_NIL/thylakoids and Au_planar/thylakoids was also investigated. DET based amperometric measurements with light ON/OFF intervals were performed initially, and afterwards electrodes were immersed into buffer and stored in the fridge for 1 day, 3 days and 7 days at 4 °C. Upon the storage in the fridge new amperometric measurements were performed and current decrease in % was calculated (Supporting Table S1). The results showed that microholes of NIL electrodes seem to have no influence on the storage stability, as the current decrease for NIL and planar electrodes was almost identical. The capacitance of biomodified NIL electrodes was evaluated by charge/discharge experiments, *i.e.*, electrodes were allowed to charge upon illumination until a relatively stable OCP was reached and subsequently discharged with a resistor. Apparently, NIL electrode modified with thylakoids provides a capacitance value of 34 F m^{-2} (Supporting Fig. S5), however, OCP was increasing with time due to the photoinduced damage of bioelements [40].

3.3. Evaluation of dual-feature photobioanode

In order to enhance charge storing capabilities, biomodified NIL electrodes were combined with a planar gold electrode modified with PEDOT, which was synthesized by cyclic voltammetry, wherein 3 cycles gave optimal capacitance/charge transfer resistance ratio (Supporting Fig. S6). Thus, dual-feature electrode containing charging/solar energy converting part (Au_NIL/thylakoids) and capacitive/charge storing part (Au_planar/PEDOT) were assembled. The construction and functional principle of dual-feature photobioanode are shown in Supporting Fig. S7. Dual-feature anodes were investigated using single potential amperometry in the presence of the mediator, Fig. 2C. More than two times higher currents compared to Au_NIL/thylakoids were achieved due to faradaic charge accumulation within the conductive polymer film. Dual feature electrodes were also tested by charge/discharge cycling under continuous illumination, as well as at day light conditions. The capacitance of the dual-feature anode (58 F m^{-2}) increased approximately twice compared to the capacitance of charging part upon artificial illumination (Fig. 3A). Photobioanode was also examined at day light conditions, resulting in almost similar capacitance value equal to 55 F m^{-2} (Fig. 3B). Noteworthy, the conductive polymer contributed to a notably lower OCP value of photobioanodes, *viz.* −0.21 V, which is crucial for the construction of high voltage photo-biodevices. Moreover, usage of the PEDOT layer resulted in stable OCP of photobioanode as low value equal to −0.21 V remained constant with time upon charge/discharge cycling, which was not the case when only the charging part, Au_NIL/thylakoids, were evaluated (Supporting Fig. S5). Interestingly, the OCP values of separate components, *i.e.* charging and capacitive parts (Fig. 4), were significantly higher, but upon electrical connection a rapid decrease was observed. The flow of photosynthetic electrons obviously accumulates at PEDOT modified capacitive part giving a strong negative charge to the dual-feature electrode. Further experiments were performed both upon artificial illumination and at day light.

3.4. Evaluation of photoelectric biosupercapacitor

For the construction of transparent and capacitive biocathode flexible ITO coated PET was covered with ITOnps. Nanostructuration with ITOnps contributed to the significant increase of the electrode capacitance, however, the expected decrease was observed upon the electrode biomodification (Supporting Fig. S8). After immobilisation of *Mv*BOx the biocathode was evaluated by charge/discharge cycling (Supporting Fig. S9) delivering a stable OCP value of 0.51 V in air saturated electrolyte and capacitance equal to 57 F m^{-2}. Finally, thylakoid based dual

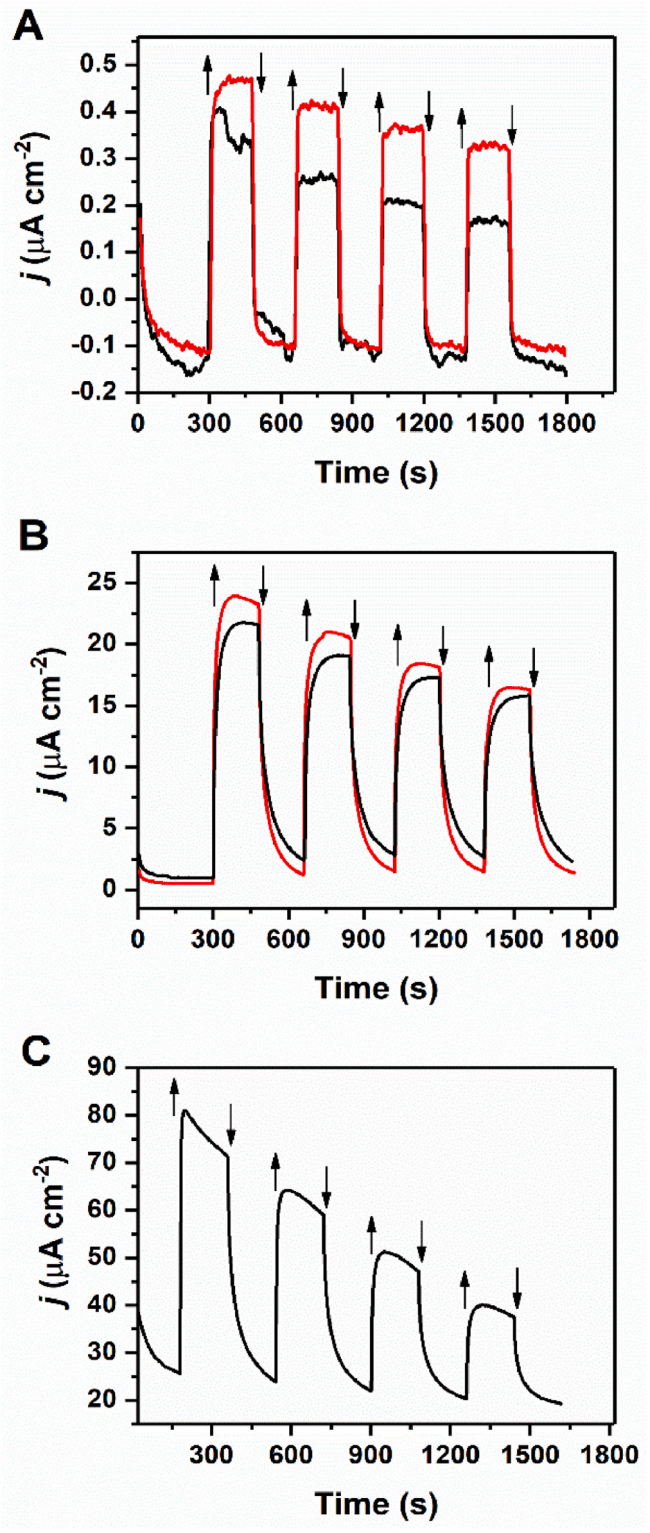

Fig. 2. Amperometric responses at 0.32 V *vs*. Ag|AgCl|KCl_{sat} of Au_planar/thylakoids, Au_NIL_thylakoids and dual feature anode. A) Direct electron transfer based amperometry; black line – Au_planar/thylakoids, red line – Au_NIL/thylakoids. B) Mediated electron transfer based amperometry recorded in the presence of 0.6 mM PBQ in the electrolyte; black line – Au_planar/thylakoids, red line – Au_NIL/thylakoids. C) Mediated electron transfer based amperometry of dual feature anode recorded in the presence of 0.6 mM PBQ in the electrolyte. ↑ and ↓ represent "light ON" and "light OFF" situations respectively. Light intensity 400 W m^{-2}. (For interpretation of the references to colour in this figure legend, the reader is referred to the Web version of this article.)

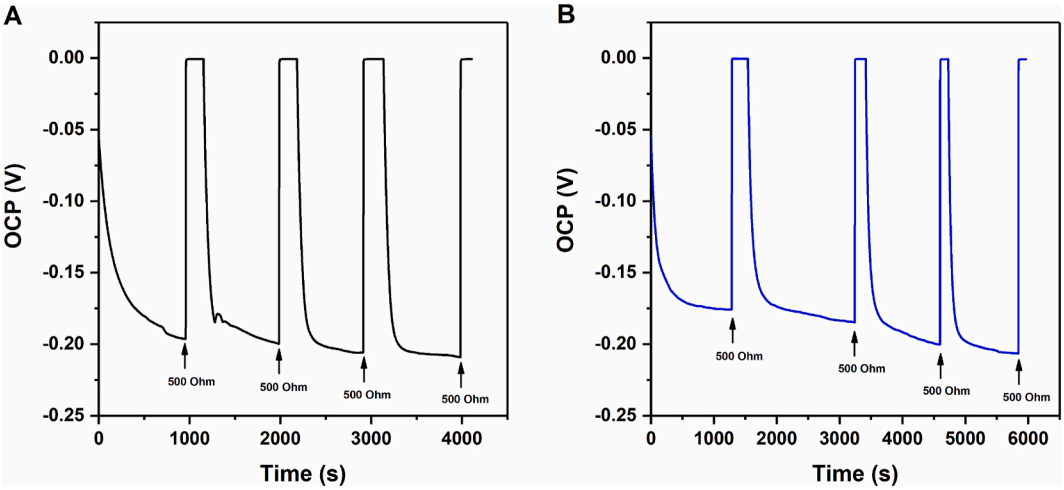

Fig. 3. Charge-discharge cycles of dual-feature anode upon illumination with light intensity 400 W m^{-2} (A) and at day light (B).

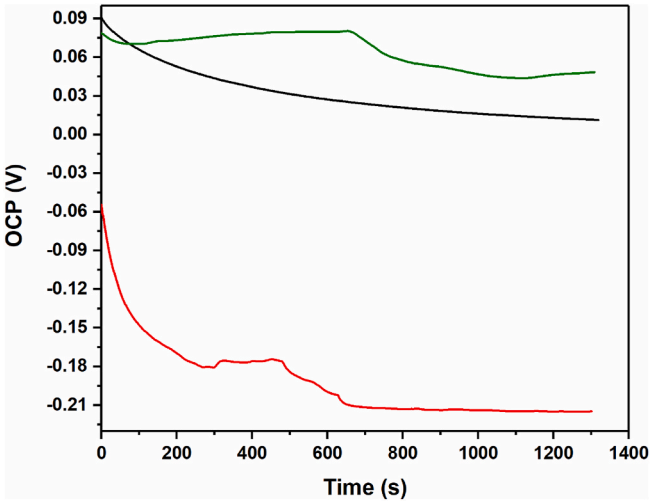

Fig. 4. OCPs of dual-feature anode and its components measured at ambient light conditions. Red line – dual feature anode, black line – Au_planar/PEDOT, green line – Au_NIL/thylakoids. (For interpretation of the references to colour in this figure legend, the reader is referred to the Web version of this article.)

feature anodes were combined with ITO/ITOnps/*Mv*BOx biocathode to design a photoelectric biosupercapacitor, the schematic representation of the device is shown in Supporting Fig. S10. The biodevice provided an OCV of 0.74 V upon continuous illumination at 400 W m^{-2}, one of the highest values for biosolar cells reported so far [11,41,42], and open-circuit voltage of the biodevice was stable upon charge/discharge cycling delivering a capacitance of 31 F m^{-2} (Fig. 5A). The device produced power output of 1 μW (0.2 W m^{-2}) at an operating voltage of 0.34 V (Fig. 6). The biosupercapacitor was also tested at day light conditions giving the same OCV value equal to 0.74 V, which was stable upon charge/discharge cycling (Fig. 5B). Power output of the device at ambient light was expectedly lower, *viz.*, 0.5 μW (0.1 W m^{-2}), Fig. 6, with a quite similar capacitance equal to 23 F m^{-2}.

4. Conclusions

In this work we have developed a dual-feature anode, composed of NIL Au electrode modified with thylakoid membranes (charging part) and planar gold electrode coated with conductive polymer PEDOT (capacitive part), functional at day light conditions. Dual feature anode, stable upon charge discharge cycling, provided OCP values as low as −0.21 V and capacitance values close to 60 F m^{-2} upon artificial illumination and at ambient light conditions. Combination of dual feature anode with transparent ITO/ITOnps electrode modified with *Mv*BOx, resulted in a photoelectric biosupercapacitor functional both at day light

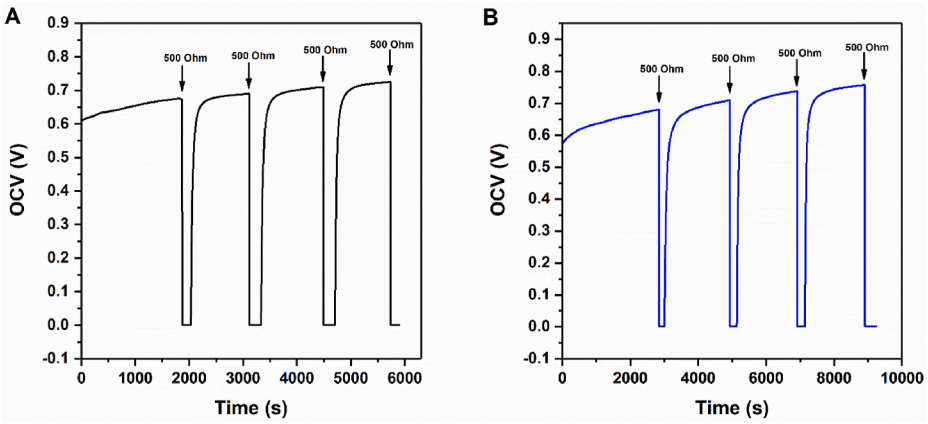

Fig. 5. Charge-discharge cycles of photo-biosupercapacitor upon illumination with light intensity 400 W m^{-2} (A) and at ambient light (B).

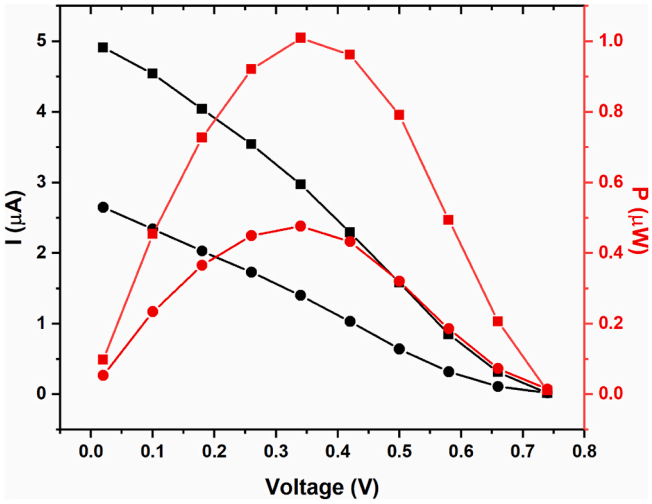

Fig. 6. Power output (red) and polarisation (black) curves of photo-biosupercapacitor obtained upon illumination with light intensity 400 W m^{-2} (squares) and at day light (circles). (For interpretation of the references to colour in this figure legend, the reader is referred to the Web version of this article.)

and upon illumination without presence of any redox mediator. The device provided a remarkably stable OCV value of 0.74 V and delivered power outputs of 0.5 μW (0.1 W m^{-2}) at ambient light conditions and 1 μW (0.2 W m^{-2}) upon illumination with artificial light source at an operating voltage of 0.34 V. The capacitance value of the device operating at day light conditions and upon illumination using the artificial light was equal to 23 F m^{-2} and 31 F m^{-2}, respectively. This study can be considered as a promising step towards fabrication of highly capacitive photo-biodevices for sustainable electricity production and storage for real applications, *i.e.*, for their use at day light conditions.

CRediT authorship contribution statement

O. Aleksejeva: Conceptualization, Methodology, Validation, Formal analysis, Investigation, Writing – original draft, Writing – review & editing. **N. Nilsson:** Methodology, Resources, Writing – original draft. **V. Genevskiy:** Investigation, Writing – original draft. **K. Thulin:** Methodology, Resources, Writing – review & editing. **S. Shleev:** Funding acquisition, Project administration, Supervision, Writing – review & editing.

Declaration of competing interest

The authors declare that they have no known competing financial interests or personal relationships that could have appeared to influence the work reported in this paper.

Acknowledgements

This work was supported financially by the Swedish Knowledge Foundation (20170168).

Appendix A. Supplementary data

Supplementary data to this article can be found online at https://doi.org/10.1016/j.jpowsour.2021.230677.

References

[1] M. Rasmussen, S.D. Minteer, Photobioelectrochemistry: solar energy conversion and biofuel production with photosynthetic catalysts, J. Electrochem. Soc. 161 (2014) H647–H655.
[2] N. Sekar, R.P. Ramasamy, Recent advances in photosynthetic energy conversion, J. Photochem. Photobiol., A C 22 (2015) 19–33.
[3] K. Hasan, R.D. Milton, M. Grattieri, T. Wang, M. Stephanz, S.D. Minteer, Photobioelectrocatalysis of intact chloroplasts for solar energy conversion, ACS Catal. 7 (2017) 2257–2265.
[4] A.J. McCormick, P. Bombelli, R.W. Bradley, R. Thorne, T. Wenzel, C.J. Howe, Biophotovoltaics: oxygenic photosynthetic organisms in the world of bioelectrochemical systems, Energy Environ. Sci. 8 (2015) 1092–1109.
[5] D. Pankratov, G. Pankratova, T.P. Dyachkova, P. Falkman, H.-E. Aakerlund, M. D. Toscano, Q. Chi, L. Gorton, Supercapacitive biosolar cell driven by direct electron transfer between photosynthetic membranes and CNT networks with enhanced performance, ACS Energy Lett 2 (2017) 2635–2639.
[6] M. Edelman, A.K. Mattoo, D1-protein dynamics in photosystem II: the lingering enigma, Photosynth. Res. 98 (2008) 609–620.
[7] J.O. Calkins, Y. Umasankar, H. O'Neill, R.P. Ramasamy, High photo-electrochemical activity of thylakoid-carbon nanotube composites for photosynthetic energy conversion, Energy Environ. Sci. 6 (2013) 1891–1900.
[8] S. Liu, P.-h. Zhang, Y. Qiu, J. Zhang, D.-y. Yu, The photoelectric properties of thylakoid membrane from two plants fabricated on nano-ZnO, Hai Yang Ke Xue 36 (2012) 50–55.
[9] H. Kanso, G. Pankratova, P. Bollella, D. Leech, D. Hernandez, L. Gorton, Sunlight photocurrent generation from thylakoid membranes on gold nanoparticle modified screen-printed electrodes, J. Electroanal. Chem. 816 (2018) 259–264.
[10] G. Pankratova, D. Pankratov, K. Hasan, H.-E. Aakerlund, P.-A. Albertsson, D. Leech, S. Shleev, L. Gorton, Supercapacitive photo-bioanodes and biosolar cells: a novel aroach for solar energy harnessing, Adv. Energy Mater. 7 (2017).
[11] G. Pankratova, D. Pankratov, C. Di Bari, A. Goni-Urtiaga, M.D. Toscano, Q. Chi, M. Pita, L. Gorton, A.L. De Lacey, Three-dimensional graphene matrix-supported and thylakoid membrane-based high-performance bioelectrochemical solar cell, ACS Appl. Energy Mater. 1 (2018) 319–323.
[12] N. Yang, Y. Zhang, J.E. Halpert, J. Zhai, D. Wang, L. Jiang, Granum-like stacking structures with TiO2-graphene nanosheets for improving photo-electric conversion, Small 8 (2012) 1762–1770.
[13] D. Ryu, Y.J. Kim, S.I. Kim, H. Hong, H.S. Ahn, K. Kim, W. Ryu, Thylakoid-deposited micro-pillar electrodes for enhanced direct extraction of photosynthetic electrons, NANOMATERIALS-BASEL 8 (2018).
[14] D. Pankratov, R. Sundberg, J. Sotres, D.B. Suyatin, I. Maximov, S. Shleev, L. Montelius, Scalable, high performance, enzymatic cathodes based on nanoimprint lithography, Beilstein J. Nanotechnol. 6 (2015) 1377–1384.
[15] Y.-P. Chen, Y.-P. Lee, J.-H. Chang, L.A. Wang, Fabrication of concave gratings by curved surface UV-nanoimprint lithography, J. Vac. Sci. Technol. B 26 (2008) 1690–1695.
[16] S. Patole, C. Vasilev, O. El-Zubir, L. Wang, M.P. Johnson, A.J. Cadby, G.J. Leggett, C.N. Hunter, Interference lithographic nanopatterning of plant and bacterial light-harvesting complexes on gold substrates, Interface Focus 5 (2015) 20150005.
[17] L. Liu, Y. Zhang, W. Wang, C. Gu, X. Bai, E. Wang, Nanosphere lithography for the fabrication of ultranarrow graphene nanoribbons and on-chip bandgap tuning of graphene, Adv. Mater. 23 (2011) 1246–1251.
[18] M.M. Alkaisi, K. Mohamed, in: M. Wang (Ed.), Three-dimensional Patterning Using Ultraviolet Curable Nanoimprint Lithography, Lithography, InTech, Croatia, 2010, pp. 572–596.
[19] S. Murthy, M. Falcon, S.V. Sreenivasan, D. Dance, S-FIL Technology: Cost of Ownership Case Study, Emerging Lithographic Technologies IX, International Society for Optics and Photonics, 2005, pp. 964–975.
[20] S.V. Sreenivasan, C.G. Willson, N.E. Schumaker, D.J. Resnick, Low-cost Nanostructure Patterning Using Step and Flash Imprint Lithography, Nanostructure Science, Metrology, and Technology, International Society for Optics and Photonics, 2002, pp. 187–194.
[21] X. Li, J. Shao, H. Tian, Y. Ding, X. Li, Fabrication of high-aspect-ratio microstructures using dielectrophoresis-electrocapillary force-driven UV-imprinting, J. Micromech. Microeng. 21 (2011) 1–9.
[22] J. Shao, X. Chen, X. Li, H. Tian, C. Wang, B. Lu, Nanoimprint lithography for the manufacturing of flexible electronics, Sci. China Technol. Sci. 62 (2019) 175–198.
[23] K.J. Morton, G. Nieberg, S. Bai, S.Y. Chou, Wafer-scale patterning of sub-40 nm diameter and high aspect ratio (>50:1) silicon pillar arrays by nanoimprint and etching, Nanotechnology 19 (2008) 1–6.
[24] L.J. Guo, Recent progress in nanoimprint technology and its applications, J. Phys. D Appl. Phys. 37 (2004) R123–R141.
[25] H. Schift, Nanoimprint lithography: an old story in modern times? A review, J. Vac. Sci. Technol. B 26 (2008) 458–480.
[26] J.-H. Chang, F.-S. Cheng, C.-C. Chao, Y.-C. Weng, S.-Y. Yang, L.A. Wang, Direct imprinting using soft mold and gas pressure for large area and curved surfaces, J. Vac. Sci. Technol., A 23 (2005) 1687–1690.
[27] J.L. Martin, B.J. Norris, E. Murphy, J.A. Crowe, Medical device development: the challenge for ergonomics, Appl. Ergon. 39 (2008) 271–283.
[28] R. Patesson, E. Brangier, X. Bollen, M. Tummers, in: S. Bagnara, R. Tartaglia, S. Albolino, T. Alexander, Y. Fujita (Eds.), How to Implement a High-Fidelity Prototyping Approach in a Cardiac Surgery Device?, Springer International Publishing, 2019, pp. 291–302.
[29] D. Pankratov, Z. Blum, D.B. Suyatin, V.O. Popov, S. Shleev, Self-charging electrochemical biocapacitor, ChemElectroChem 1 (2014) 343–346.
[30] G. Pankratova, D. Pankratov, K. Hasan, H.-E. Aakerlund, P.-A. Albertsson, D. Leech, S. Shleev, L. Gorton, Supercapacitive photo-bioanodes and biosolar cells: a novel approach for solar energy harnessing, Adv. Energy Mater. 7 (2017).
[31] E. Andreasson, P. Svensson, C. Weibull, P.A. Albertsson, Separation and characterization of stroma and grana membranes - evidence for heterogeneity in

antenna size of both photosystem I and photosystem II, Biochim. Biophys. Acta Bioenerg. 936 (1988) 339–350.
[32] D.I. Arnon, Copper enzymes in isolated chloroplasts. Polyphenoloxidase in Beta vulgaris, Plant Physiol. 24 (1949) 1–15.
[33] Z.W. Zhong, X.C. Shan, Y.C. Yao, Investigation of antiadhesive coatings for nanoimprinting lithography, Mater. Manuf. Process. 25 (2010) 658–664.
[34] I. Horcas, R. Fernandez, J.M. Gomez-Rodriguez, J. Colchero, J. Gomez-Herrero, A. M. Baro, WSXM: a software for scanning probe microscopy and a tool for nanotechnology, Rev. Sci. Instrum. 78 (2007) 1–8.
[35] L.M. Fischer, M. Tenje, A.R. Heiskanen, N. Masuda, J. Castillo, A. Bentien, J. Emneus, M.H. Jakobsen, A. Boisen, Gold cleaning methods for electrochemical detection applications, Microelectron. Eng. 86 (2009) 1282–1285.
[36] D. Pankratov, J. Sotres, A. Barrantes, T. Arnebrant, S. Shleev, Interfacial behavior and activity of laccase and bilirubin oxidase on bare gold surfaces, Langmuir 30 (2014) 2943–2951.
[37] E. Gonzalez-Arribas, O. Aleksejeva, T. Bobrowski, M.D. Toscano, L. Gorton, W. Schuhmann, S. Shleev, Solar biosupercapacitor, Electrochem. Commun. 74 (2017) 9–13.
[38] X. Xiao, M. Wang, H. Li, P. Si, One-step fabrication of bio-functionalized nanoporous gold/poly(3,4-ethylenedioxythiophene) hybrid electrodes for amperometric glucose sensing, Talanta 116 (2013) 1054–1059.
[39] K. Hasan, Y. Dilgin, S.C. Emek, M. Tavahodi, H.-E. Aakerlund, P.-A. Albertsson, L. Gorton, Photoelectrochemical communication between thylakoid membranes and gold electrodes through different quinone derivatives, ChemElectroChem 1 (2014) 131–139.
[40] A. Melis, Photosystem-II damage and repair cycle in chloroplasts: what modulates the rate of photodamage, Trends Plant Sci. 4 (1999) 130–135.
[41] M. Riedel, J. Wersig, A. Ruff, W. Schuhmann, A. Zouni, F. Lisdat, A Z-scheme-inspired photobioelectrochemical H2O/O2 Cell with a 1 V open-circuit voltage combining photosystem II and PbS quantum dots, Angew. Chem. Int. Ed. 58 (2019) 801–805.
[42] M. Masi, P. Bollella, M. Riedel, F. Lisdat, E. Katz, Photobiofuel cell with sustainable energy generation based on micro/nanostructured electrode materials, ACS Appl. Energy Mater. 3 (2020) 9543–9549.